PAPER

Check for updates

Vertically aligned PANI nanorod arrays grown on graphene oxide nanosheets for a high-performance NH₃ gas sensor†

Jinwei Wei,‡[a] Bo Liang,‡[a] Qingpeng Cao,[a] Chentian Mo,[a] Youming Zheng[b] and Xuesong Ye [ID] *[ac]

In this paper, vertically aligned PANI nanorod arrays were successfully prepared on GO nanosheets at low temperature *via* a dilute polymerization method, in which the GO nanosheets with abundant hydrophilic groups were employed to support the heterogeneous growth of uniformly-distributed PANI nanorod arrays. The acquired nanocomposite was characterized by scanning electron microscopy (SEM), transmission electron microscopy (TEM), Fourier transform infrared spectroscopy (FTIR), Raman spectroscopy, and X-ray photoelectron spectroscopy (XPS). NH₃ sensing performances of the as-prepared nanocomposite were carefully examined. With the help of the enhanced synergistic effect derived from the large number of p–n heterojunctions in the deliberately-designed microstructure, the device exhibited an enhanced response to NH₃ vapor (14.63 at 50 ppm), wide dynamic range (1–6400 ppm), and fast response and recovery processes, in comparison to pure PANI nanofibers. The impact of the drop-coating amount of the sensing nanocomposite on the sensing performances was also investigated to find out the suitable amount for fabricating a high-performance ammonia sensor. Herein, the superior performances of the proposed well-organized microstructure make it an effective nanocomposite for gas sensing applications.

Introduction

Gas sensors based on graphene and its derivatives, such as graphene oxide (GO) and reduced graphene oxide (RGO), have caught more and more attention, since the first demonstration of individual gas molecule detection using graphene as a sensitive material.[1] This trend, to a great extent, is due to the amazing properties of graphene as a two-dimensional atomic crystal of sp² bonded carbon, which has been successfully used in supercapacitor electrode materials,[2,3] electronic devices[4] and gas sensors.[5,6]

[a]*Biosensor National Special Laboratory, College of Biomedical Engineering and Instrument Science, Zhejiang University, Hangzhou 310027, PR China. E-mail: yexuesong@zju.edu.cn; Fax: +86 0571 87952756; Tel: +86 0571 87951090*

[b]*Department of Technical Information, Zhejiang Provincial Museum, Hangzhou 310007, PR China*

[c]*State Key Lab of CAD&CG, Zhejiang University, Hangzhou 310027, PR China*

† Electronic supplementary information (ESI) available: SEM images of PNrA/GO synthesized at different concentrations of aniline; TEM images of PNrA/GO synthesized with different reaction times; gas response behaviors based on graphene oxide to 50 ppm NH₃; gas sensitivity of PNrA/GO (1.3 : 1) to NH₃ at 50, 100, 200 and 400 ppm; dynamic response and its polynomial fitting of the ammonia sensor to different concentrations of NH₃; gas sensing behaviors of the ammonia sensor to various interfering gas species; gas sensitivity changes of sensor S1 and S2 under various RH levels; sensitivity changes of the ammonia sensor under various working temperatures. See DOI: 10.1039/c7ra04636g

‡ These authors contributed equally to this work.

At present, more efforts have been made to decorate graphene or GO with functional nanomaterials for higher sensitivity and better selectivity in gas sensors. The decoration of CVD grown graphene with gold nanoparticles using the galvanic displacement method has been proposed for H₂S monitoring.[7] In addition, metal oxide nanomaterials were combined with graphene for gas sensor fabrication with excellent gas sensing properties. A high performance NO₂ gas sensor has been successfully fabricated using ZnO and Au nanoparticles modified reduced graphene oxide ternary hybrids, showing high sensitivity, fast response and recovery rate.[8] Another NO₂ gas sensor with a high sensitivity and low detection of level has been achieved by using self-assembled graphene/polymer composite nanofibers as sensitive material.[9]

Among all the functional nanomaterials exploited for sensitivity enhancement, conducting polymers such as polyaniline (PANI), polypyrrole and polythiophene presented excellent synergistic effect when introduced into graphene or RGO based gas sensors.[10,11] There have been a number of scientific reports on graphene/PANI nanocomposite used in gas sensor fabrication, which is largely attributed to the facile synthesis and environmental stability of PANI. Graphene/PANI nanocomposite synthesized by chemical oxidation polymerization was used for NH₃ determination, showing a wide linear range of concentrations from 1 to 6400 ppm.[12] Besides, PANI with fibrous morphology in the graphene/PANI nano-composite has been achieved to develop a novel H₂ sensor.[13] Despite some

improvements of sensing performances, the inherent agglomeration of graphene in chemical synthesis processes, due to high surface energy, was very difficult to overcome if not impossible. Therefore, few well-organized microstructures of graphene/PANI nanocomposites have been achieved yet.

Although various graphene/PANI or RGO/PANI nano-composites were successfully exploited in gas sensor fabrications[12,13] and supercapacitor electrodes,[2,3,14] little attention, to the best of our knowledge, has been paid to the facile chemical synthesis of well-organized GO/PANI nano-composite and its gas sensing performances. Here, we presented a controllable *in situ* polymerization method for vertically aligned PANI nanorod arrays (PNrA) grown on GO nanosheets (PNrA/GO) at low temperature.[15,16] It suggested that GO nanosheets with abundant hydroxyl and carboxyl groups could provide active nucleation sites for PANI growth, leading to a relatively uniform distribution in PANI nanorod arrays. Therefore, the as-fabricated ammonia sensor, with the proposed sensitive nano-composite and a well-organized micro-structure design, exhibited greater overall performances, such as higher sensitivity and wider detection range, than those of PANI/RGO based gas sensors reported previously.[11,17,18]

Experimental section

Characterizations

For morphologic characterization, both the prepared nano-composites and gas sensor architectures were observed by field-emission scanning electron microscopy (FESEM, Hitachi SU8010) with the accelerating voltage ranging from 0.1 to 30 kV. Transmission electron microscopy (TEM) characterization was made on a JEOL JEM-1200EX electron microscopy with an accelerating voltage of 200 kV. For chemical composition analysis, Fourier transform infrared spectra (FT-IR) of GO, PANI nanofibers, and the synthesized PNrA/GO were recorded by Tensor 27 from Bruker with the wavenumber range of 7800 cm^{-1} to 400 cm^{-1}. Raman spectra were obtained using a Lab-RAM HR Evolution system with a 532 nm wavelength laser, which was bought from Horiba Jobin Yvon. The XPS spectra of the products were detected by VG ESCALAB MARK II spectrometer with the energy resolution to be 0.8 eV.

Materials

Graphene oxide (GO) powder was purchased from Nanjing XFNANO Materials Tech Co., Ltd. (Nanjing, China). Ammonium persulfate (APS) was obtained from Aladdin Ltd. (Shanghai, China). All other reagents were purchased from Sinopharm Chemical Reagent Co., Ltd. (Shanghai, China) and were reagent grade. Deionized (18 MΩ cm^{-1}) water was used for all aqueous solutions.

Preparation of vertically aligned PANI nanorod arrays on GO nanosheets

The successful preparation was accomplished by *in situ* dilute polymerization of aniline for vertically aligned PANI nanorod arrays uniformly-distributed on graphene oxide nanosheets (abbreviated as PNrA/GO).

In detail, our approach for PNrA/GO can be presented as follows: 21.6 mg of GO was dispersed in 15 mL of deionized water with the assistance of powerful ultrasonication for 0.5 h, obtaining a brown solution. Then 83.82 mg of aniline was mixed with 22.5 mL of $HClO_4$ (1.0 M), followed by magnetic stirring for 0.5 h at room temperature. And 136.88 mg of APS was dispersed in 22.5 mL of $HClO_4$ (1.0 M) with continuous stirring, followed by cold storage for 0.5 h at 0 °C. Afterwards, the obtained GO dispersed solution was rapidly added to the aniline mixture and the resulting mixture was treated with magnetic stirring for another 0.5 h at 0 °C. The APS solution was then rapidly mixed with the above GO/aniline mixture and the resulting suspension with an aniline concentration of 0.015 M, a ratio of [aniline]/[GO] to be 3.9 : 1 and a ratio of [aniline]/[APS] to be 1.5 : 1 was treated by magnetic stirring for 24 h at 0 °C. For comparison, the PNrA/GO were also successfully prepared in suspensions with a ratio of [aniline]/[GO] to be 5.2 : 1, 2.6 : 1 and 1.3 : 1, in which the aniline concentration was 0.02 M, 0.01 M and 0.005 M, respectively and the ratio of [aniline]/[APS] remained unchanged. Thus, the obtained PNrA/GO nano-composites were denoted as PNrA/GO (5.2 : 1), PNrA/GO (3.9 : 1), PNrA/GO (2.6 : 1) and PNrA/GO (1.3 : 1), respectively. After the polymerization process, centrifugal purification was employed to remove the remaining reactants and other by-products. For further comparison, the pure PANI nanofibers and PANI nanofibers/GO nano-composite were polymerized in 0.1 M aniline solution in the absence and presence of GO nanosheets by the same approach as mentioned above, and thus the prepared products were respectively named as PNF and PNF/GO for short.

To illustrate the growth process of the nanocomposite, the PNrA/GO synthesized in suspensions with the aniline concentration of 0.015 M, a ratio of [aniline]/[GO] to be 3.9 : 1 and a ratio of [aniline]/[APS] to be 1.5 : 1 was prepared at the reaction time of 1 h, 4 h, 8 h and 24 h.

Fabrication of gas sensor and the evaluation of sensing properties

After purification, PNrA/GO achieved good stability and uniform dispersion in aqueous state at room temperature to greatly facilitate the sensor fabrication processes. Then, the as-prepared ammonia gas sensor was obtained by drop-coating the PNrA/GO onto the interdigitated electrodes, followed by thermal treatment in vacuum oven at 45 °C for 8 h. The inter-digitated electrodes was fabricated on Si/SiO$_2$ substrate with the size of 4.3 mm × 4.0 mm × 1.0 mm, and both the width and gaps between the gold lines were 3 μm. In comparison, the ammonia sensor based on pure PANI nanofibers, GO nano-sheets and PANI nanofibers/GO composite were fabricated using the same method as mentioned above, respectively.

Then, gas sensing evaluations were conducted by recording the relative real-time resistance changes when the gas sensor were exposed to different concentrations of NH_3 at room temperature. The typical testing procedures can be conducted

as follows: firstly, the gas sensor was kept still in the air till the resistance response reached its steady state, where the resistance was recorded as R_{air}; then, the sensor was immediately opposed to ammonia diluted in a specific concentration using N_2 as carrier gas, and we assigned the resistance here as R_{gas}; thirdly, it was withdrawn out to the surrounding air after that the R_{gas} got its equilibrium state. The standard NH_3 (50 000 ppm, N_2 as carrier gas) and pure N_2 were purchased from MINXINGQITI (Hangzhou, China) and different concentrations of NH_3 can be easily and accurately obtained by using Sabio Gas Dilution Calibrator (Model 4010L, USA). Additionally, the resistance of the as-fabricated interdigitated electrodes were recorded and stored using digital multimeter (Agilent 34410A, USA), which was connected to PC by USB to RS232 serial port cable.

It is noted that the sensor response of ammonia sensor is defined as $S = ((R_{gas} - R_{air})/R_{air})$, in which the R_{gas} represents the resistance in target gas and the R_{air} for that in air as mentioned above. Moreover, the response time is defined as the consumed time at which the magnitude reaches 90% of the total response signal and the recovery time denotes the time required for a sensor to restore 90% of the total resistance change.

Results and discussion

Characterization of vertically aligned PANI nanorod arrays on graphene oxide

Here, a low-temperature dilute polymerization method was utilized to grow vertically aligned PANI nanorod arrays on GO nanosheets and the acquired nanocomposite was drop-coated onto the interdigitated electrodes for gas sensor fabrication. Scanning electron microscopy (SEM) images were collected to characterize the surface morphology of PNrA/GO and pure PANI nanofibers, respectively. Fig. 1a and b revealed that the dilute-polymerized vertically aligned PANI nanorod arrays with the crystal height to be several tens of nanometers were uniformly distributed on the graphene oxide nanosheets. In comparison, Fig. 1c and d revealed that pure PANI nanofibers and PANI nanofibers/GO composite were successfully synthesized with the removal and addition of GO nanosheets and that the homogeneous polymerization of aniline monomers dominated the main process when the aniline concentration was raised up to 0.1 M, leading to randomly interconnected PANI nanofibers.

Moreover, it was observed that electrode gaps were covered by several layers of PNrA/GO on the as-fabricated ammonia sensor (Fig. 1e). It has been clearly revealed in the high magnification Fig. 1f that graphene oxide nanosheets were decorated with tightly-arranged perpendicular PANI nanorod arrays.
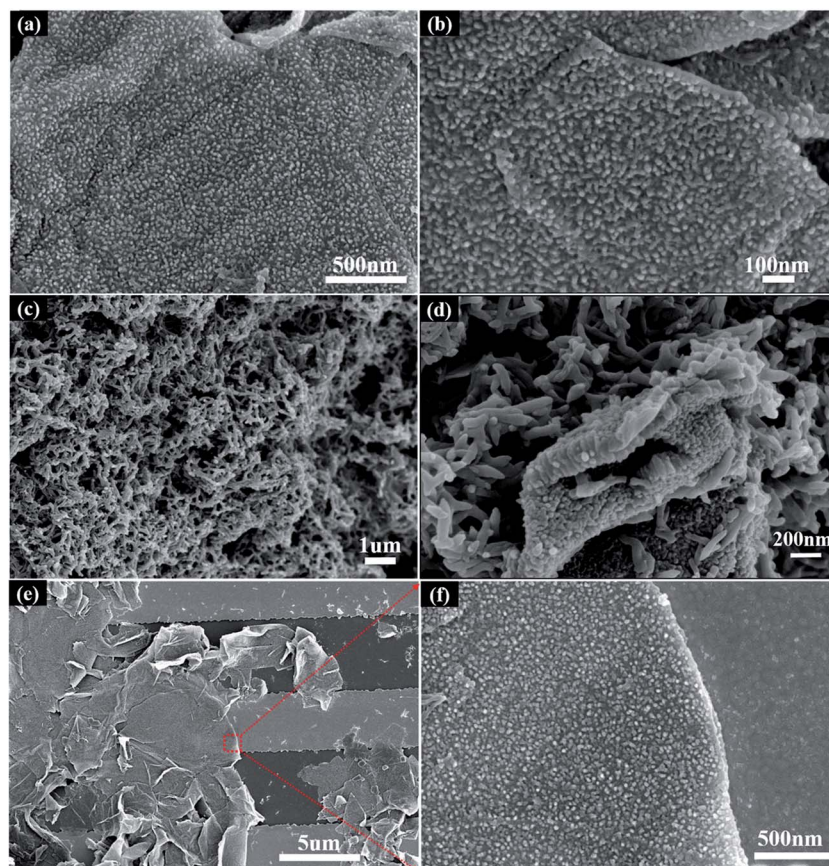

Fig. 1 (a) Low and (b) high magnification SEM images of vertically aligned PANI nanorod arrays grown on GO nanosheets (PNrA/GO). (c) SEM image of pure PANI nanofibers in interconnected network (PNF). (d) SEM image of PANI nanofibers synthesized with GO (PNF/GO). (e) Low and (f) high resolution SEM image of the ammonia sensor by drop-coating the as-prepared PNrA/GO onto interdigitated electrodes.

On the basis of the above investigation, a detailed formation mechanism of PNrA/GO nanocomposite was further illustrated in Fig. S1.† In chemical polymerization of PANI, two possible nucleation mechanism, namely homogeneous nucleation and heterogeneous nucleation, coexist and compete with each other. Particularly, homogeneous nucleation usually dominates the process in high-concentration bulk solution, resulting in interconnected PANI nanofibers as shown in Fig. 1c and d, and yet the heterogeneous nucleation does in solution with foreign seeds or at the interface between GO and bulk solution. In Fig. S1b–d,† the homogeneous polymerization was greatly suppressed in dilute aniline solution (0.015 M for Fig. S1b, 0.01 M for Fig. S1c and 0.005 M for Fig. S1d†) where a super-saturation state cannot be reached. Besides, the presence of abundant hydrophilic groups on GO nanosheets can attach to the anilinium ions *via* electrostatic attraction and serve as active nucleation sites for heterogeneous polymerization. The active sites would also minimize the interfacial energy barrier between the GO nanosheets and aniline solution, which was beneficial for the subsequent growth of PANI nanorod arrays on GO.

Besides, much longer and thicker PANI nanorod arrays appeared when the aniline concentration increased from 0.005 M to 0.015 M, which would enhance the nanocomposite's sensing performances. However, the homogeneous growth also happened if the aniline concentration reached 0.02 M, and several segments of PANI nanowires and PANI nanorods agglomeration can be found on GO nanosheets in Fig. S1a,† showing a strong tendency to form PANI thin film and PANI nanofibers.

To further characterize the heterogeneous growth of PNrA/GO nanocomposite, different samples were taken out from the reaction solution at reaction time of 1 h, 4 h, 8 h and 24 h. Fig. 2a revealed the schematic illustration of the heterogeneous nucleation and growth process of PNrA/GO at different reaction periods. And as shown in Fig. 2b, the attracted anilinium ions on GO nanosheets behaved as the nucleation sites to reduce the interfacial energy and the whole Gibbs free energy which facilitated further polymerization, and yet most areas of GO nanosheets remained smooth due to the slow reaction speed at low temperature. Fig. 2c showed the increased nucleation seeds and
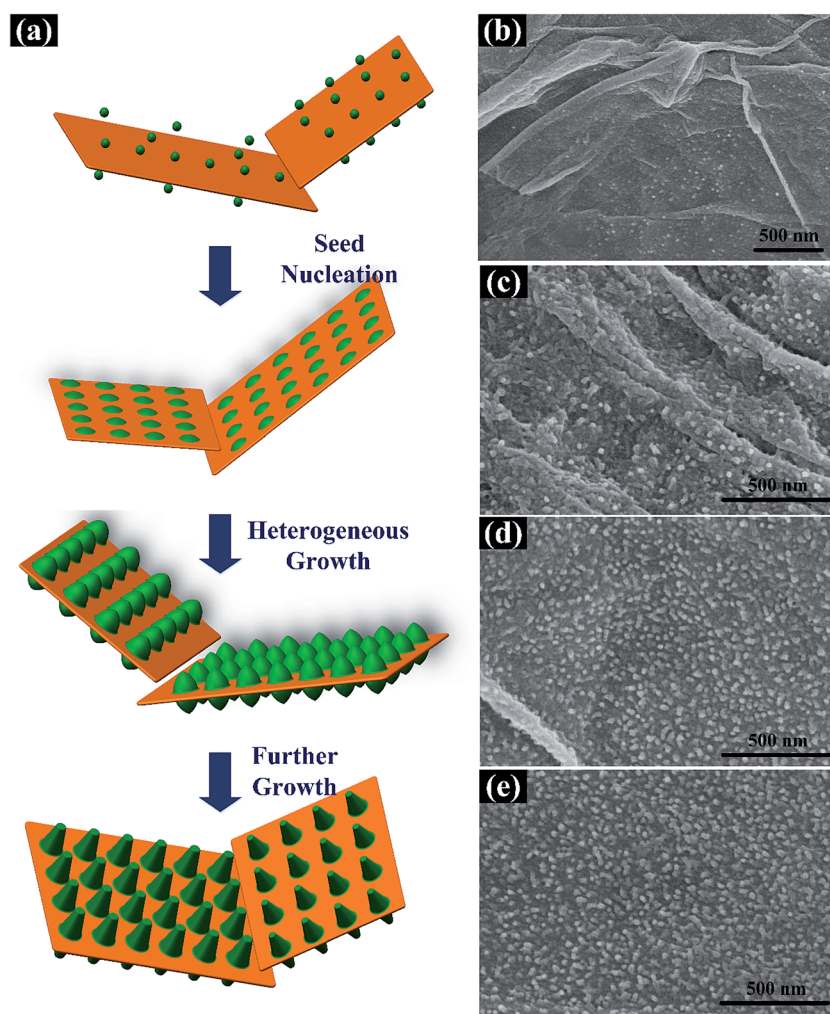

Fig. 2 (a) Schematic illustration of the heterogeneous nucleation and growth process of PNrA/GO at different reaction periods. And SEM images of PNrA/GO obtained at different reaction periods: (b) 1 h; (c) 4 h; (d) 8 h; (e) 24 h.
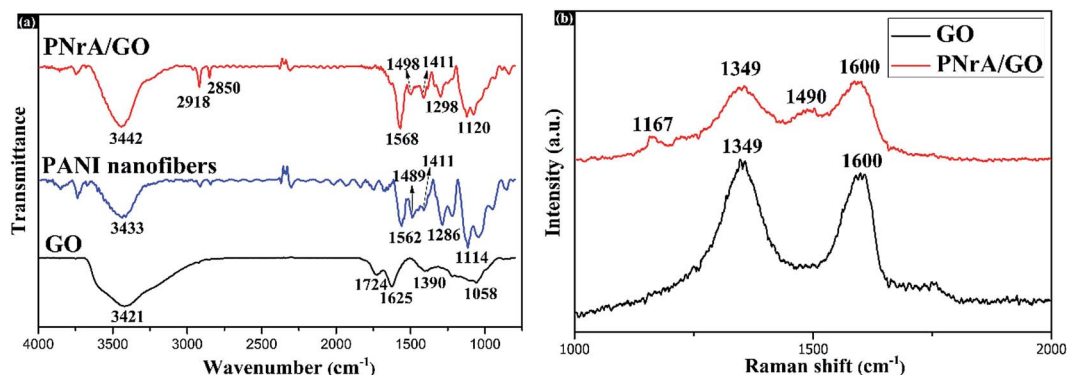
Fig. 3 (a) FTIR spectra of GO, PANI nanofibers and the as-prepared PNrA/GO (from bottom to top). (b) Raman spectra of GO and the as-prepared PNrA/GO (from bottom to top).

the gradually-grown PANI nanoparticles on GO nanosheets. In the successive process as Fig. 2d and e, the dispersed PANI nanoparticles developed into vertically aligned PANI nanorod arrays with uniform distribution on GO nanosheets, and the as-prepared nanocomposite showed no appearance of particle-like PANI aggregates because of the dilute aniline. No PANI nanofibers was found due to the great homogeneous suppression effect in the dilute aniline solution. TEM images of the samples (1 h, 4 h, 8 h and 24 h) were also collected in Fig. S2† to characterize the heterogeneous polymerization processes. It was demonstrated that PANI gradually developed from sparse nanoparticles (Fig. S2a†) into denser and longer rod-like nanoarrays (Fig. S2d†).

The functional groups in the nanocomposite were further investigated by FTIR spectroscopy. In the FTIR spectrum of GO (Fig. 3a), the peaks at 3421, 1724, 1625, 1390 and 1058 cm^{-1} were attributed as the characteristic vibrations of the hydroxyl group, C=O in COOH, intercalated water, O=C–O from carboxylate, and C–O in C–OH/C–O–C functional groups, respectively.[19] In the case of pure PANI nanofibers, the peaks at

1562 and 1489 cm^{-1} were characterized to be the C=C stretching vibrations in the quinoid and benzenoid units of PANI, respectively. And the peaks at 1286 and 1114 cm^{-1} were correspondingly attributed as the C–N stretching vibrations in the quinoid and benzenoid units. Compared with GO, the appearance of characteristic peaks at 2918 and 2850 cm^{-1} in PNrA/GO were demonstrated as the successful insertion of PANI oligomers into GO layers. Also, the distinct spectrum shown in pure PANI nanofibers were found in the PNrA/GO, further proving the combination of PANI nanostructures with GO nanosheets. It was noted that the peaks at 1724, 1390 and 1058 cm^{-1} disappeared in the prepared nanocomposite, which was attributed to the ion bonding behavior between anilinium cation ($C_6H_5NH_3^+$) and COO^-/CO^- radicals of GO.[20,21]

Structural investigation was sequentially carried out by Raman spectra, which is displayed in Fig. 3b. For all the samples, the distinctive peaks for D band (1349 cm^{-1}) and G band (1600 cm^{-1}) were observed for GO. Otherwise, the weaker D band and G band obtained for PNrA/GO could be due to the well coverage of PANI on GO nanosheets.[22] In comparison, the
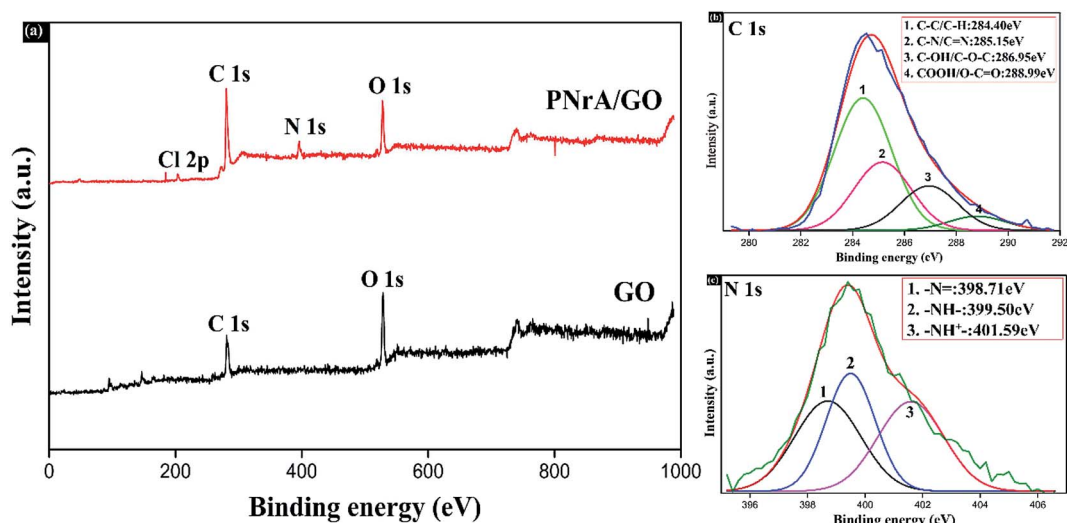

Fig. 4 (a) XPS spectra of GO and the as-prepared PNrA/GO (from bottom to top). High resolution XPS spectra and the fitting curves of (b) C 1s and (c) N 1s in the PNrA/GO.

appearance of two characteristic peaks located at 1167 and 1490 cm^{-1} was in accordance with the C–N stretching vibrations in the benzenoid units (1114 cm^{-1}) and the C=C stretching vibrations in the benzenoid units (1489 cm^{-1}) of PANI in the FTIR spectrum as shown in Fig. 3a. And it demonstrated the existence of PANI in the as-synthesized nanocomposite. Furthermore, the C–N stretching vibrations in the benzenoid units of PANI shifted to higher wavenumbers from 1114 cm^{-1} of pure PANI nanofibers to 1167 cm^{-1} in PNrA/GO nanocomposite, which indicated the π–π conjugated interaction between PANI and GO nanosheets.

XPS characterization was broadly treated as an effective method to analyze the elemental composition and surrounding chemical states for functional nanomaterials. In the wide range spectra of Fig. 4a, both GO and the resulting PNrA/GO exhibited two strong peaks at 284.6 eV and 529.1 eV corresponding to the appearance of C 1s and O 1s, respectively. Meanwhile, the existence of N 1s and Cl 2p peaks was demonstrated in the PNrA/GO, indicating the presence of PANI, which was doped with HClO$_4$. From the high resolution scanning spectrum for C 1s in Fig. 4b, it was observed that the binding energy at 284.40 eV, 285.15 eV, 286.95 eV and 288.99 eV, derived from Gaussian fit, were reasonably attributed to the C–C group, C–N or C=N groups in PANI frameworks, C–OH or C–O–C groups in graphene oxide, and the COOH components, respectively. Also, the high resolution of N 1s spectrum was deconvoluted into three Gaussian peaks (Fig. 4c) with the binding energy at 398.71 eV, 399.50 eV and 401.59 eV, which indicated the presence of benzenoid amine (=N–), quinoid amine (–NH–) and the nitrogen cationic radical (–NH$^+$–), respectively. In particular, the slight shifts of binding energy as observed in Fig. 4b and c were largely due to π–π conjugated stacking between the PANI frameworks and graphene oxide nanosheets. Additionally, the obtained XPS results revealed that the PANI nanorod arrays in the nanocomposite were in high-level doped state, which was in agreement with the good conductivity measured in the initial state.

Evaluation of gas sensing properties

As a toxic and corrosive chemicals widely existed in chemical industry, ammonia gas, especially in high concentrations, poses a great threat to human health, thus generating a strong urge for highly sensitive and selective ammonia gas sensor. Therefore, the as-prepared PNrA/GO here in a novel micro-structure was employed as sensitive material for ammonia sensor application.

The relative resistance changes of the as-fabricated gas sensors were then recorded when different gas concentrations were imposed on them. The typical gas response behaviors of the four ammonia gas sensors based on GO, PNF, PNF/GO and PNrA/GO nanocomposites towards NH$_3$ vapor at various concentrations ranging from 50 ppm to 400 ppm were illustrated as Fig. 5a. It is widely known that PANI gas sensor will transform from the emeraldine salt form (conductive state) to its emeraldine base one (insulating one) on exposure to NH$_3$ atmosphere, in which NH$_3$ molecules display a strong deprotonation effect, leading the localization of polarons of conducting PANI and thus a dramatic decrease in conductance.[23] The deprotonation process is reversible, and the conductive state will restore with the decomposition of the PANI and NH$_3$ molecules after the injection of fresh air. Conversely, a magnified view of GO-based gas sensor in Fig. S3† generated a slight decrease of resistance, showing n-type semiconducting properties in NH$_3$ atmosphere, which can be attributed to the increased electron carrier concentration in GO nanosheets by the electron donating effect of NH$_3$ molecules. In addition, the PNF/GO nanocomposite reveal enhanced sensing response to the analyte compared to GO nanosheets or pure PANI nanofibers. Actually, the p-type PANI nanofibers can interact with the n-type semiconducting GO nanosheets through electrostatic attraction, hydrogen bonding and π–π electron stacking and thus p–n heterojunctions in the nanocomposite were formed for improved sensing performance.[24-26] And it also demonstrated the highest response of PNrA/GO was obtained among those of all the nanocomposites. The enhanced synergistic effect between PANI and GO can be derived here from the larger number of PANI–GO heterojunctions, since the PANI nanorod arrays are synthesized in a uniform distribution on the GO nanosheets compared to PANI nanofibers/GO hybrid.[12] And with regards to the decreased hole carrier concentration on exposure to the analyte, there would be an increase of depletion layer between PANI nanorod arrays and GO nano-sheets, which leads to reduced conducting pathways and enhanced sensing characteristics.[27] Additionally, the vertically-grown PANI nanorod arrays will facilitate gas molecule diffusion process, which enable rapid and reversible adsorption and desorption kinetics with short response and recovery period. Hence, the as-prepared PNrA/GO can be an ideal candidate for constructing a high-performance ammonia sensor with higher sensitivity and other required properties.

To illustrate the detailed sensing mechanism, the influence of vertically aligned PANI nanorod arrays on the ammonia sensing response was demonstrated in Fig. 5b by comparing the sensing performances of different weight ratio of aniline to GO in as-synthesized nanocomposites. Fig. S4,† a magnified view of PNrA/GO (1.3 : 1) in Fig. 5b, showed the similar negative response behaviors as that of pure GO nanosheets in Fig. S3,† which means sparse PANI nanoparticles have little positive effect and that GO dominate the sensing performance in the nanocomposite. In contrast, the PNrA/GO (5.2 : 1) in which the aniline concentration was raised to a high level, exhibited the similar sensing response just as that of PNF/GO in Fig. 5a. The trend here can be demonstrated to be in accordance with the morphological structure changes shown in Fig. S1.† Additionally, more interaction heterojunctions between PANI and GO were generated by the longer and thicker PANI nanorod arrays distributed on GO achieved in PNrA/GO (3.9 : 1) and thus the derived stronger synergistic effect lead to higher sensing response, compared to that of PNrA/GO (2.6 : 1). Therefore, the PNrA/GO (3.9 : 1) was chosen for other evaluations in the following sections, and a short name of PNrA/GO was taken for convenience.
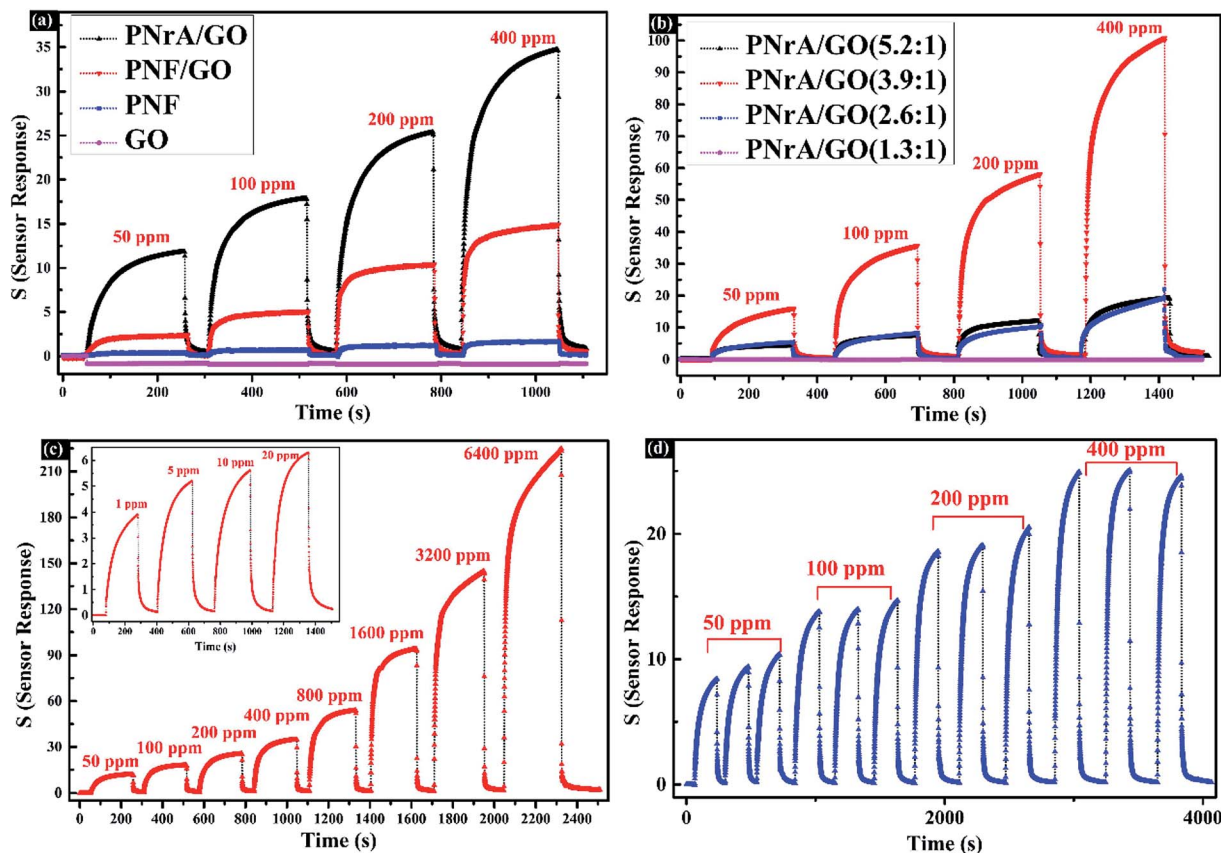
Fig. 5   (a) Gas response behaviors based on graphene oxide (GO), PANI nanofibers (PNF), PANI nanofibers/GO composite (PNF/GO) and the as-prepared PNrA/GO towards 50, 100, 200 and 400 ppm of NH$_3$ in sequence at room temperature. (b) Gas sensitivity on exposure to 50, 100, 200 and 400 ppm NH$_3$ of PNrA/GO synthesized at different weight ratio of aniline to GO: 5.2 : 1, 3.9 : 1, 2.6 : 1 and 1.3 : 1. And the inset is a magnified view of PNrA/GO (1.3 : 1) to NH$_3$. (c) Gas sensing performance of the PNrA/GO based ammonia sensor upon exposure to different concentration of NH$_3$ ranging from 1 ppm to 6400 ppm. Inset is the transient responses to 1, 5, 10 and 20 ppm of NH$_3$. (d) Gas sensing repeatability of the ammonia sensor based on PNrA/GO to 50, 100, 200 and 400 ppm of NH$_3$.

In order to further investigate the detailed properties, the dynamic responses of PNrA/GO to NH$_3$ gas at various concentrations ranging from 1 ppm to 6400 ppm were evaluated in Fig. 5c. It showed the resistance of the as-prepared sensor experienced a sharp increase at 50 ppm (sensor response of 14.63 to NH$_3$) with the response time to be 61 s and recovery time as short as 10 s after sensor withdrawal. Dynamic range is always regarded as one of the most significant parameters for physical or chemical sensors. The fitting data of the response toward ammonia concentration ranging from 50 ppm to 6400 ppm (Fig. S5†) shows the experimental data fits well with a two order polynomial ($R^2 = 0.997$), which meant the fabricated ammonia sensor has a great potential for quantitative gas analysis in this concentration range.[28] In summary, the sensing performances of ammonia sensor based on PNrA/GO were compared in Table 1 with other ammonia sensors previously reported.[29,30] It revealed that the prepared ammonia sensor exhibited a relatively higher sensitivity and wider detection range.

As illustrated as Fig. 5d, the repeatability of the ammonia sensor was examined on exposure to the same gas concentration of 50, 100, 200 and 400 ppm in multiple cycles. And

a satisfactory performance in repeatability was achieved from the consistency of the ascending and descending curves, indicating an unchanged adsorption and desorption kinetics at different times.

In Fig. 6a, the impact of the drop-coating amount of the PNrA/GO on the sensing performances were carefully investigated in three ammonia sensors prepared by first dispersing the nanocomposite with deionized water in different volume ratio as 1 : 1, 1 : 10 and 1 : 20, and then drop-coating the same amount of diluted product onto the electrode. Here, the as-fabricated ammonia sensors were named as PNrA/GO_1X, PNrA/GO_10X and PNrA/GO_20X, respectively. The highest gas sensitivity was obtained for PNrA/GO_20X, and yet the sensing behavior showed great nonlinearity to higher concentration of the ammonia vapor. With the decrease of the drop-coating amount, the nanocomposite stacked layers assembled on the electrode surface were gradually reduced to facilitate the interactions between the analyte with the inner composite layer, which made a great difference to the sensor response. In contrast, the PNrA/GO_1X exhibited a slower response and recovery behaviors, resulting in a slight upward baseline. And this was largely attributed to the slow diffusion of gas molecules

Table 1 The comparison of the sensing performances between the as-fabricated ammonia sensor and other previously reported sensors

Sensitive materials	Working temperature (°C)	Surface morphology	Sensor response to 50 ppm NH_3	Detection range (ppm)	Response/recovery time (s)	Ref.
RGO/PANI	RT[a]	Nanosheets/nanoparticles	0.6	5–50	500/240	11
Graphene/PANI	RT	Nanosheets/nanofibers	4.7	1–6400	50/23	12
RGO/SnO$_2$/PANI	25	RGO@SnO$_2$/PANI nanocomposite	1.5	10–50	600/1200	17
CeO$_2$/PANI	RT	Core–shell CeO$_2$@PANI	6.5	2–400	57.6/360	27
TiO$_2$/PPy/GN	RT	Nanoparticle@PPy/graphene	1.02	1–200	36/16	30
PANI/GO	RT	PANI nanorod arrays/GO	14.63	1–6400	61/10	This work

[a] RT means room temperature here.

in the severe stacked layers of the nanocomposite. In summary, PNrA/GO_10X showed greater overall sensing performances when the sensitivity and detection range were balanced for optimizing the drop-coating amount of the sensing material to construct a high-performance gas sensor.

The selectivity of the prepared ammonia sensor was then demonstrated in Fig. 6b and S6† by exposing it to different gas species at 50 ppm, including C$_2$H$_4$, CH$_4$, C$_4$H$_8$, H$_2$S, H$_2$ and SO$_2$,

and that the sensor response to 50 ppm NH_3 was analyzed to be 14.63, much higher than that of other gas species (0.38 of C$_2$H$_4$, 1.02 of CH$_4$, 1.18 of C$_4$H$_8$, 0.7 of H$_2$S, 0.92 of H$_2$ and 0.15 of SO$_2$). Generally, each gas species, due to their different molecule structures and the resultant interactions with the sensing nanocomposite, can produce different response mechanisms including protonation, deprotonation, reduction, swelling and conformational alignment.[23] And the preferable selectivity
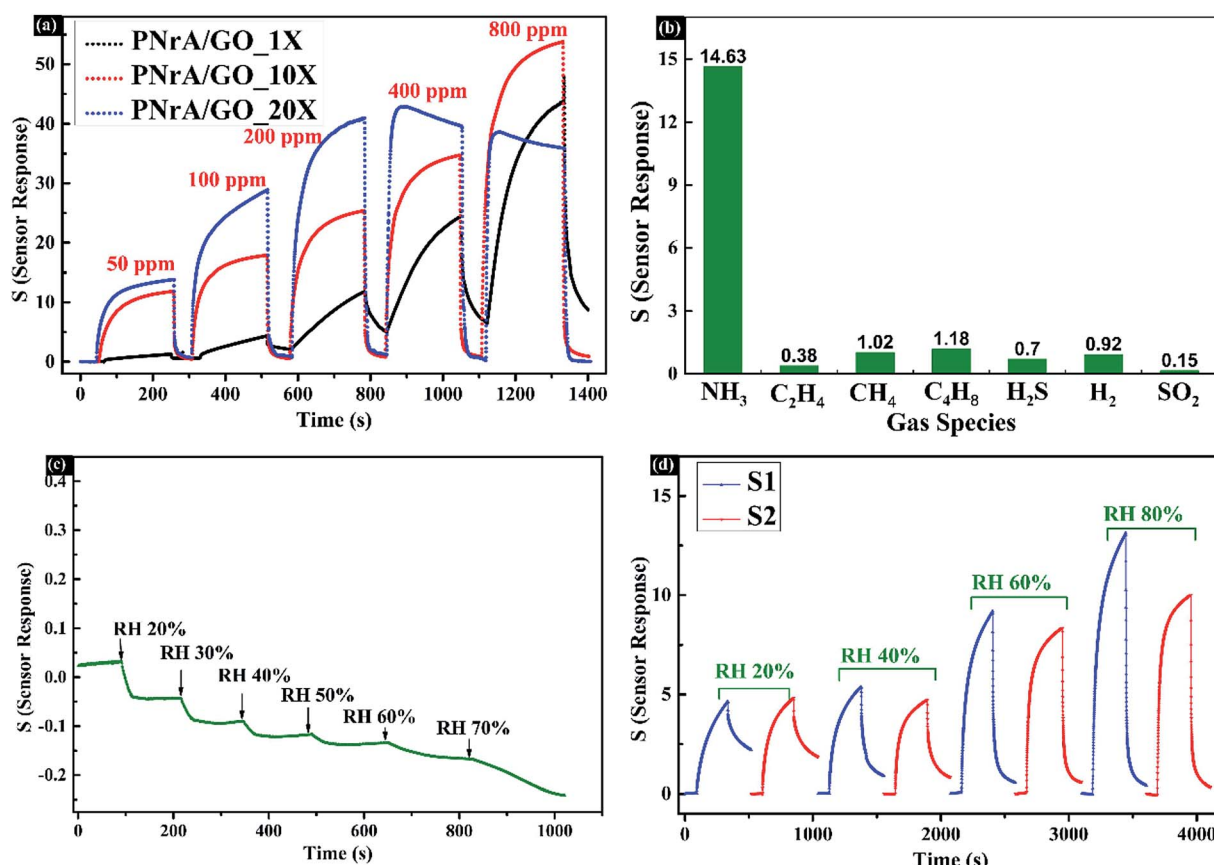

Fig. 6 (a) Gas sensing behaviors to 50, 100, 200, 400 and 800 ppm of NH$_3$ of PNrA/GO diluted by deionized water in different volume ratio as 1 : 1, 1 : 10 and 1 : 20 (named as PNrA/GO_1X, PNrA/GO_10X and PNrA/GO_20X, respectively). (b) Gas sensing selectivity of the ammonia sensor to various interfering gas species at concentration of 50 ppm, including C$_2$H$_4$, CH$_4$, C$_4$H$_8$, H$_2$S, H$_2$ and SO$_2$. (c) Sensor response behaviors of PNrA/GO based ammonia sensor under different relative humidity levels. (d) Gas sensing behaviors of PNrA/GO based ammonia sensor (sensor S1 and sensor S2 were fabricated in the same batch) to 50 ppm of NH$_3$ under different RH levels ranging from 20% to 80%.
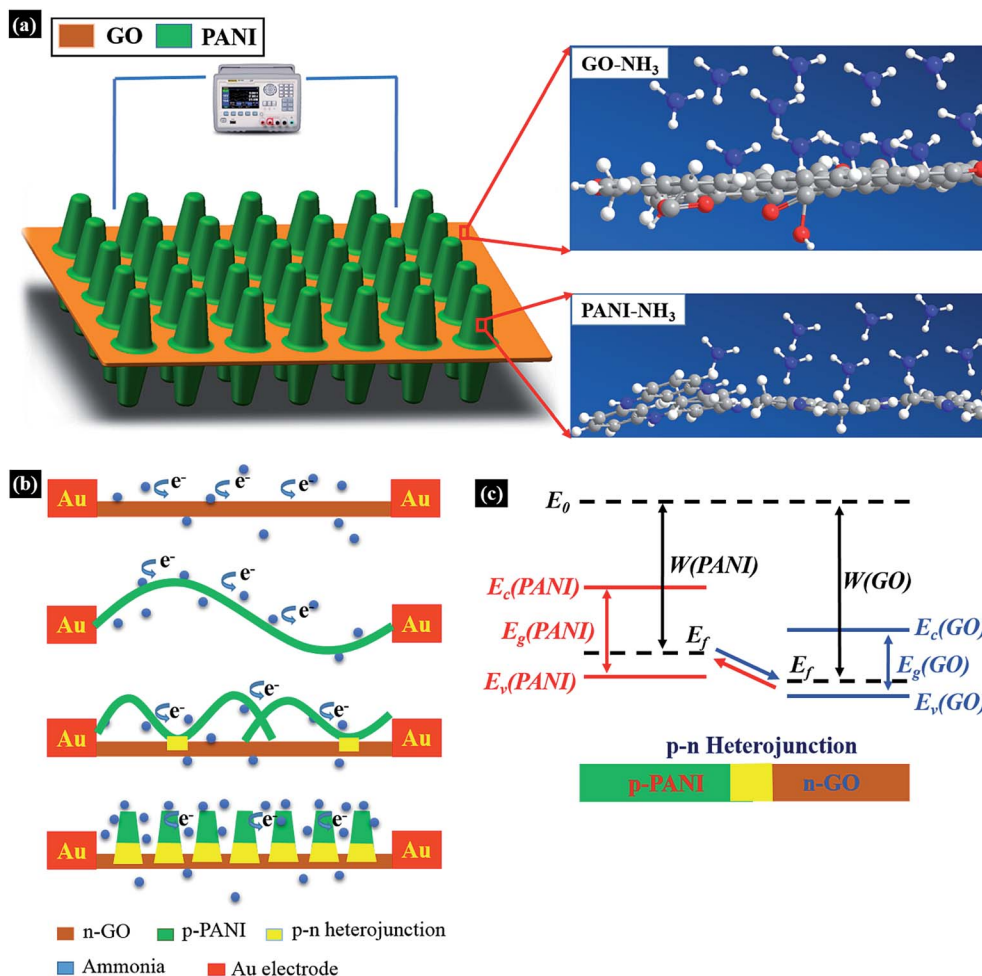
Fig. 7 (a) Schematic illustration of the interactions between PNrA/GO and NH_3 molecules at room temperature. (b) Formation and modulation mechanism of PANI/GO n–p heterojunction in NH_3 atmosphere. (c) Schematic energy band diagram of p-type PANI and n-type GO (E_0 is vacuum energy level, E_f is Fermi energy level, E_c is the bottom of conduction band and E_v is the top of valence band).

performance of the proposed PNrA/GO was largely attributed to the stronger deprotonation effect of NH_3 to PANI in contrast to other interfering gases. Besides, the contradiction of desired selectivity and acceptable recovery time was compromised due to the simultaneous achievement of reversible deprotonation/ protonation reactions and specific chemical adsorption of NH_3 molecules to PANI. Additionally, Fig. 6c revealed minor impacts on the sensor resistance changes caused by relative humidity at different levels from RH 20% to RH 70%. However, different response patterns were clearly observed in Fig. 6d when gas sensor was exposed to 50 ppm NH_3 at different RH%. In detail, both the two sensors fabricated in the same batch (abbreviated as S1 and S2) exhibited lower sensitivity in low RH% as 20% and 40%, and yet higher RH% impose positive effects on the sensor response (Fig. S7†). Therefore, humidity compensation should be adopted when the sensor was used at different RH%. Moreover, the influence of working temperature on sensing performances was carefully investigated in Fig. S8.† It clearly revealed that the sensitivity of the as-fabricated ammonia sensor gradually decreased with the increase of the surrounding temperature from 10 °C to 70 °C. It suggested that

further efforts should be made to relieve the negative influences caused by humidity and temperature on the sensing characteristics.

Sensing mechanism analysis

Schematic illustration of the interactions between the nano-composite and ammonia molecules at room temperature was revealed in Fig. 7a, where enhanced sensing response could be attributed to the effect of large number of p–n hetero-junctions formed in the well-organized PNrA/GO nano-composite. The interaction of NH_3 with graphene oxides containing the hydroxyl and epoxy functional groups has been carefully investigated in first-principles calculations and experimental observations.[24,31] It showed that great charge transferred from NH_3 to GO when the adsorbed NH_3 molecules on GO were decomposed into chemisorbed NH_2 species as a result of the H atom abstraction, and that the introduction of nitrogen func-tionalities converted the insulating GO to n-type GO and nar-rowed the band gap.[26,32] The n-type GO can also be observed in Fig. S3† where the resistance obviously decreased upon

exposure to NH$_3$. In contrast, the hole concentration in positively charged PANI backbone was reduced by electron-donating NH$_3$ molecules due to the dedoping reaction. And in this case, the p-type PANI transform from the emeraldine salt form (conductive state) to its emeraldine base one (insulating one). Therefore, p–n heterojunctions were formed in the PANI/GO nanocomposite when exposed to the NH$_3$ atmosphere.

To further understand synergistic effect of the heterojunction, the modulation mechanism and energy band diagram of PANI/GO junction was illustrated in Fig. 7b and c. The band gaps of p-type PANI and n-type GO were 2.8 eV (ref. 27) and 2.2 eV,[26] respectively, and a p–n heterojunction was formed at the interface of PANI and GO, due to the different Fermi energy level. In the case of PANI nanofibers/GO composite, carrier transportation could find pathways in inter-chain or intra-chain PANI backbones, and heterojunctions formed between PANI nanofibers and GO may slightly enhance the sensing performance compared to bare PANI nanofibers. When the PANI nanorod arrays were uniformly distributed on GO nanosheets, enhanced synergistic effect was derived from the larger number of p–n heterojunctions and the depletion region in the nano-composite may be increased by NH$_3$ electron-donating and energy band modulation effect, which greatly blocked the carrier conducting pathways and attributed to the excellent sensing responses.

Conclusions

Vertically aligned PANI nanorod arrays could be facilely synthesized via an in situ dilute polymerization method with aniline molecules as precursors and GO nanosheets as soft support. The homogenous growth of PANI was greatly suppressed in ultralow concentrations, which made uniformly distributed PANI nanorod arrays grow on GO in a heterogeneous way. An ammonia gas sensor based on the resulting composite was then successfully fabricated. Compared with other nanocomposites based ammonia sensors, it exhibited excellent sensitivity, wider dynamic range to NH$_3$ of 1 ppm to 6400 ppm, short response and recovery time of several tens of seconds, as well as favorable selectivity when exposed to other disturbing gases. Here, the large number of p–n heterojunctions between PANI and GO in the strategically designed microstructure enhanced the synergistic effect, and contributed to these remarkable characteristics of the sensor. Besides, the most suitable drop-coating amount of the nano-composite was demonstrated to achieve the desired sensing performances. In general, effective methods for new microstructure design and sensor fabrication optimization will pave a new way for further improvements to high-performance gas sensor.

Acknowledgements

Notes and references

1 F. Schedin, A. K. Geim, S. V. Morozov, E. W. Hill, P. Blake, M. I. Katsnelson and K. S. Novoselov, Nat. Mater., 2007, 6, 652–655.

2 D. Ghosh, S. Giri, M. Mandal and C. K. Das, RSC Adv., 2014, 4, 26094–26101.

3 S. Giri, D. Ghosh and C. K. Das, Adv. Funct. Mater., 2014, 24, 1312–1324.

4 F. Schwierz, Nat. Nanotechnol., 2010, 5, 487–496.

5 H. Choi, J. S. Choi, J.-S. Kim, J.-H. Choe, K. H. Chung, J.-W. Shin, J. T. Kim, D.-H. Youn, K.-C. Kim, J.-I. Lee, S.-Y. Choi, P. Kim, C.-G. Choi and Y.-J. Yu, Small, 2014, 10, 3685–3691.

6 F. Yavari and N. Koratkar, J. Phys. Chem. Lett., 2012, 3, 1746–1753.

7 A. Gutes, B. Hsia, A. Sussman, W. Mickelson, A. Zettl, C. Carraro and R. Maboudian, Nanoscale, 2012, 4, 438–440.

8 S. Liu, Z. Wang, Y. Zhang, Z. Dong and T. Zhang, RSC Adv., 2015, 5, 91760–91765.

9 W. J. Yuan, L. Huang, Q. Q. Zhou and G. Q. Shi, ACS Appl. Mater. Interfaces, 2014, 6, 17003–17008.

10 S. Bai, Y. Zhao, J. Sun, Y. Tian, R. Luo, D. Li and A. Chen, Chem. Commun., 2015, 51, 7524–7527.

11 X. Huang, N. Hu, R. Gao, Y. Yu, Y. Wang, Z. Yang, E. S.-W. Kong, H. Wei and Y. Zhang, J. Mater. Chem., 2012, 22, 22488–22495.

12 Z. Wu, X. Chen, S. Zhu, Z. Zhou, Y. Yao, W. Quan and B. Liu, Sens. Actuators, B, 2013, 178, 485–493.

13 L. Al-Mashat, K. Shin, K. Kalantar-zadeh, J. D. Plessis, S. H. Han, R. W. Kojima, R. B. Kaner, D. Li, X. Gou, S. J. Ippolito and W. Wlodarski, J. Phys. Chem. C, 2010, 114, 16168–16173.

14 X. Feng, N. Chen, J. Zhou, Y. Li, Z. Huang, L. Zhang, Y. Ma, L. Wang and X. Yan, New J. Chem., 2015, 39, 2261–2268.

15 D. Shao, G. Hou, J. Li, T. Wen, X. Ren and X. Wang, Chem. Eng. J., 2014, 255, 604–612.

16 S. Zhang, M. Zeng, W. Xu, J. Li, J. Li, J. Xu and X. Wang, Dalton Trans., 2013, 42, 7854–7858.

17 Z. Ye, Y. Jiang, H. Tai, N. Guo, G. Xie and Z. Yuan, J. Mater. Sci.: Mater. Electron., 2015, 26, 833–841.

18 X. Huang, N. Hu, L. Zhang, L. Wei, H. Wei and Y. Zhang, Synth. Met., 2013, 185, 25–30.

19 S. Park, K.-S. Lee, G. Bozoklu, W. Cai, S. T. Nguyen and R. S. Ruoff, ACS Nano, 2008, 2, 572–578.

20 Y. Matsuo, T. Niwa and Y. Sugie, Carbon, 1999, 37, 897–901.

21 S.-J. Lin, H.-J. Sun, T.-J. Peng and L.-H. Jiang, High Perform. Polym., 2014, 26, 790–797.

22 Y. Luo, D. Kong, Y. Jia, J. Luo, Y. Lu, D. Zhang, K. Qiu, C. M. Li and T. Yu, RSC Adv., 2013, 3, 5851–5859.

23 S. Virji, J. Huang, R. B. Kaner and B. H. Weiller, Nano Lett., 2004, 4, 491–496.

24 S. Tang and Z. Cao, J. Phys. Chem. C, 2012, 116, 8778–8791.

25 C. Petit, M. Seredych and T. J. Bandosz, J. Mater. Chem., 2009, 19, 9176–9185.

26 T.-F. Yeh, S.-J. Chen, C.-S. Yeh and H. Teng, *J. Phys. Chem. C*, 2013, **117**, 6516–6524.

27 L. Wang, H. Huang, S. Xiao, D. Cai, Y. Liu, B. Liu, D. Wang, C. Wang, H. Li, Y. Wang, Q. Li and T. Wang, *ACS Appl. Mater. Interfaces*, 2014, **6**, 14131–14140.

28 X. Wang, S. Zhang, M. Shao, J. Huang, X. Deng, P. Hou and X. Xu, *Sens. Actuators, B*, 2017, **251**, 27–33.

29 P. Wan, X. Wen, C. Sun, B. K. Chandran, H. Zhang, X. Sun and X. Chen, *Small*, 2015, **11**, 5409–5415.

30 C. Xiang, D. Jiang, Y. Zou, H. Chu, S. Qiu, H. Zhang, F. Xu, L. Sun and L. Zheng, *Ceram. Int.*, 2015, **41**, 6432–6438.

31 E. C. Mattson, K. Pande, M. Unger, S. Cui, G. Lu, M. Gajdardziska-Josifovska, M. Weinert, J. Chen and C. J. Hirschmugl, *J. Phys. Chem. C*, 2013, **117**, 10698–10707.

32 F. Li, X. Jiang, J. Zhao and S. Zhang, *Nano Energy*, 2015, **16**, 488–515.